machines

MDPI

Article

Impact of Multiple Operating Parameters Interactions on Load Swing of Tower Cranes

Peijin Liu [1], Chong Zhao [1], Yu Sun [2,*] and Xinhui Zhang [1]

[1] School of Mechanical and Electrical Engineering, Xi'an University of Architecture and Technology, Xi'an 710055, China; liuxpj@xauat.edu.cn (P.L.); zcxjayouxiang@xauat.edu.cn (C.Z.); zxh1104216212@xauat.edu.cn (X.Z.)
[2] School of Science, Xi'an University of Architecture and Technology, Xi'an 710055, China
* Correspondence: sunlyu@xauat.edu.cn

Abstract: The mechanisms and interactive effects of multiple operating parameters of tower cranes on load swing are not yet clear, which leads to the exacerbation of load swing during the lifting process due to improper control parameter settings. To address this issue, this paper establishes an electromechanical rigid-flexible coupling (EMRFC) model for tower cranes to accurately simulate the characteristics of load swing caused by flexible transmission and electromechanical nonlinear coupling. Furthermore, the Sobol sensitivity method is used to screen out the dominant and interactive operating parameters affecting load swing, and to reveal the patterns of their impact on load swing. The results show that the stiffness of the flexible transmission system has a significant impact on the load swing, which cannot be neglected in modeling and analysis. Among the dominant operating parameters, the lifting height has the greatest effect on load swing. Lifting height, luffing speed, and slewing speed show significant interactions on load swing, and the interactions make a significant difference to the load swing in different operating phases. Finally, this paper gives the reasonable interval of operation parameters of a hoisting operation under the composite working condition, which provides a scientific basis and theoretical guidance for intelligent control of tower crane operation.

Keywords: tower crane; load swing; EMRFC model; Sobol sensitivity analysis; multiple operating parameters

check for updates

Academic Editor: Fu-Cheng Wang

Received: 16 December 2024
Revised: 19 January 2025
Accepted: 20 January 2025
Published: 23 January 2025

Citation: Liu, P.; Zhao, C.; Sun, Y.; Zhang, X. Impact of Multiple Operating Parameters Interactions on Load Swing of Tower Cranes. *Machines* **2025**, *13*, 85. https://doi.org/10.3390/machines13020085

Copyright: © 2025 by the authors. Licensee MDPI, Basel, Switzerland. This article is an open access article distributed under the terms and conditions of the Creative Commons Attribution (CC BY) license (https://creativecommons.org/licenses/by/4.0/).

1. Introduction

Tower cranes are indispensable key logistics equipment for the machinery and equipment manufacturing industry, but their lifting operations are often hampered by the load swing, which reduces lifting efficiency and accuracy [1]. At present, the impact of load swing is mainly mitigated through improvements in mechanical structures or optimization of intelligent control [2,3]. However, in the application of these two types of technologies, research on the interaction mechanisms and influencing mechanisms of the main operational parameters during the operation of tower cranes has not been deeply developed, such as the speed and acceleration of the end of the actuator, the lifting height and the lifting mass parameters. This lack of theoretical guidance and basis for the application of technology has restricted the enhancement of tower crane operational performance. Therefore, studying their impact on load swing is a prerequisite for achieving intelligent and high-precision control of tower cranes, which is of great significance for promoting the development of green intelligent construction [4].

Currently, the impact effects of tower crane operating parameters on load swing are mainly studied under single working conditions, including slewing [5], luffing [6], and lifting conditions, separately [7], or in scenarios where the discrete influences of parameters under composite working conditions are considered. Considering that tower cranes usually work under composite working conditions [8], Liu et al. studied how individual operating parameters impact load swing under slewing-lifting and luffing-lifting conditions. They analyzed the impact of these parameters on the time-frequency domain characteristics of the load swing angle. However, they did not reveal the specific contribution of different operating parameters on the load swing under the same operating conditions [9,10]. Peng [11] analyzed the impact of single operating parameters on the load swing under the slewing-luffing condition, but the tower crane is a strongly coupled system [12], the research on the interactions of operating parameters on load swing is still not effectively carried out under composite working conditions. In addition, accurate modeling of the tower crane is the basis for conducting this research. Figure 1 shows the QTZ55 tower crane, widely employed in engineering construction.



Figure 1. The QTZ55 tower crane.

Existing tower crane modeling is primarily based on rigid body dynamics models. Rigid body dynamics models treat tower crane components as rigid bodies that do not undergo flexible deformation, making these models easy to establish with faster numerical solution speeds. Cheng [13,14] developed a complex finite element model for a tower crane, obtaining the trajectory of the load in three-dimensional space. Zhang et al. [15–17] constructed a tower crane model using the assumed modal method and Lagrange equations. They determined the impact of load mass on the load swing angle, assuming linear controllability of the driving force. However, they overlooked the nonlinear impact of components, such as the influence of motors and inverters in the electrical drive system on the driving force control output, especially the torque jitter when the motor starts and stops, which increases the complexity of load swing. Therefore, it is necessary to accurately simulate the tower crane model by combining electromechanical coupling dynamics models. Florentin et al. [18] developed a tower crane model using vibration theory and dynamics equations, considering the impact of motor torque jitter on load swing. They designed a control approach to minimize load swing according to the law of load swing. They idealized the flexible drive process of the tower crane and regarded the load swing as a simple oscillating motion connected by rigid rods. However, the tower crane is a complex piece of equipment with characteristics of electromechanical coupling and rigid-flexible coupling [19,20], and its lifting action is realized by pulley groups composed of steel wire ropes to transfer power to mechanical components [21]. During the operation of the tower crane, the wire ropes are subjected to dynamic loads that vibrations, which affect the load

swing through transmission components. This complex dynamic response is difficult to simulate in conventional static mathematical models [22,23].

In response to the shortcomings, the main contributions of this study include:

(1) Using the multi-body dynamics modeling method that combines physical and mathematical models, and considering the nonlinearity of the electromechanical system and the flexibility factors of the transmission mechanisms, an Electromechanical Rigid-Flexible Coupling (EMRFC) model for tower cranes has been established. This model accurately simulates the operational characteristics of tower cranes under the coupling effects of rigidity and flexibility, as well as the mechanisms affecting the swing of loads.
(2) The Sobol sensitivity analysis method is applied to the analysis of the interactive mechanism of tower crane operation parameters, deriving the primary and interactive operation parameters that affect load swing. The study investigates the characteristics of how these tower crane operation parameters influence load swing.
(3) This paper is the first to explicitly classify tower crane operation parameters into dominant and interactive operation parameters. The methods presented can provide a scientific evaluation for the operational range of these parameters, offering a basis for the setting of trajectory intervals for intelligent control reference input signals.

The rest of the paper is structured as follows: in Section 2, the electromechanical-rigid-flexible coupling model is established, and the principle of the Sobol sensitivity method is introduced; Section 3 verifies the accuracy of the model and analyzes the influence of the wire rope elasticity on the load swing. The dominant and interactive operating parameters affecting load swing are obtained by the Sobol sensitivity method, and their influence laws on load swing are further analyzed. Section 4 summarizes the main work of this paper.

2. Modeling and Analysis Methods

2.1. Tower Crane Modeling

In this section, with the flexible transmission mechanism serving as the actuating unit and the motor drive system serving as the power unit, the electromechanical rigid-flexible coupling (EMRFC) model for the tower crane is constructed using a multibody dynamical modeling method that integrates physical modeling with mathematical modeling. The flexible transmission mechanisms, which are the rope pulley mechanisms for luffing and lifting, respectively, are composed of transmission components and flexible ropes. Considering the universality of the model, the stiffness of the steel wire rope and the servo control module within the motor drive system are represented as mathematical models, while the other parts are represented as physical models.

To highlight the key factors or variables in the paper and to ensure the generalizability of the model, the following assumptions are therefore made:

(1) Neglect the deformation of the boom and tower as well as the friction of the moving joints
(2) The radial and tangential deformation of the wire rope is ignored.
(3) There is no relative swing between the hook and the load.

The methodological framework for the EMRFC modeling is shown in Figure 2, which consists of two modules: the mechanical subsystem and the electrical subsystem. In this framework, the geometric characteristics of each rigid body are provided in the form of structural parameters by the three-dimensional (3D) structural model; the stiffness coefficient of the steel wire rope is described using mechanical equations; the drive motor is connected to the multibody dynamics model through interfaces of drive speed and load torque; the controller receives feedback speed and acceleration from the reducer motor and inputs drive voltage to the geared motor to control the motor to operate with high

precision according to the motion reference trajectory. Below is a detailed introduction to the modeling process of these two modules respectively. In addition, the complete system model built in the MATLAB 2022a/Simulink environment has been shown in Figure A1.

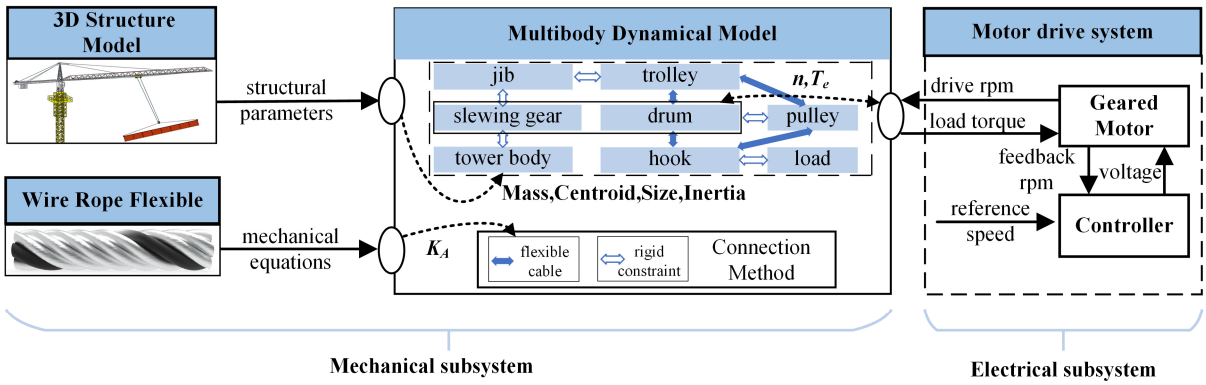


Figure 2. The methodological framework for the EMRFC modeling of the tower crane.

2.1.1. Mechanical Subsystem

1. 3D Structure Model

The 3D structure model is shown in Figure 3, including the tower body, jib, trolley, load, drum, pulley, and hook. The dimensions of the structural model are based on the actual size of the tower structure. The material used for the 3D structural model is Q235 carbon steel, and its performance parameters are presented in Table 1 of Section 3.1. To facilitate the description of the geometric relationship, the coordinates, and related parameters are defined: *OXYZ* is the three-dimensional coordinate system describing the motion position. *O* represents the slewing center, with the *Z* axis coinciding with the center axis of the tower body. The *X* axis coincides with the axis of the boom, while the *Y* axis is perpendicular to both the *X* and *Z* axes. The *X* and *Y* axes change with the movement of the jib. α and x represent the slewing angle and the luffing distance, respectively. θ_1, θ_2, S, l represent the radial swing angle, the tangential swing angle, the offset distance, and the lifting height, respectively. The offset distance is the horizontal distance between the load and the center of the trolley and contains the characteristics of the swing angle and the length of the wire rope. Meanwhile, the following assumptions are made: the tower body consists of standard sections connected rigidly, and the pulley and reel are wire rope winding objects and there is no relative sliding between them and the wire rope.

2. Wire Rope Flexible

As shown in Figure 4 wire rope model, the wire rope used has 6 strands around the core. Considering that the flexible transmission is related to the axial length of the wire rope, the main concern is the axial stiffness of the wire rope. The axial stiffness of the wire rope can be calculated according to Equations (1) and (2) [24]. The equations consider the structural layout and Poisson effect of wire ropes in lifting equipment and can accurately describe the wire rope stiffness coefficient. It is calculated as follows:

$$\begin{cases} K_{Ai} = (E_0 A_{ci} + \frac{N E_0 A_{wi} {\eta_i}^2}{\sin(\alpha_i)}) \frac{L_0}{L_i}, i = 1, 2 \\ \eta_i = \frac{\sin^2(\alpha_i) - \nu \cos^2(\alpha_i)/(1+\xi)}{1 + \frac{\nu \xi \cos^2(\alpha_i)}{1+\xi} + \frac{2(1-\nu^2)\xi^2 C_{ni} \cos^4(\alpha_i)}{(1+\xi)(1+\xi(1-\cos^2(\alpha_i)))}} \end{cases} . \quad (1)$$

where: K_{Ai} is the stiffness coefficient of the wire rope, and subscript i = 1, 2 indicates the wire rope of the lifting and luffing mechanism. N is the number of core-wound wires, and E is the elastic modulus. A_{ci} and A_{wi} are the cross-sectional area of the core and core-wound

wires. α_i is the helix angle. L_0 is the reference rope length, and L_i is the length of the transmission mechanism ($L_1 = L_0 + 2l$). ν is the Poisson's ratio, and ξ is the diameter ratio of the core. C_{ni} is the nondimensional contract compliance. Besides mechanical properties, this parameter depends on normal contact forces and stresses, body shape, load, and boundary conditions. The following equation set was derived:

$$\begin{cases} C_{ni} = D_{ei} - 1 - \ln(2P_{Ni}/(1+\sin^2(\alpha_i)\xi)) \\ P_{Ni} = A_{wi}\eta_{si}\varepsilon_{wi}(1-\nu^2)/(\pi E R_{ci} r_i) \\ \eta_{si} = (1+\xi)\cos^2(\alpha_i)/(1+\xi(1-\cos^2(\alpha_i))) \\ D_{ei} = \pi\sqrt{3}(1-2\nu)/(4(1-\nu)) - 2 - (5-4\nu)/(8(1-\nu)) - \ln(2\sqrt{3}) \end{cases} . \quad (2)$$

where: P_{Ni} is the non-dimensional contact force. ε_{wi} is the strain of the wire. D_{ei} is the deformation coefficient. r_i is the sum of the core-wire radii.

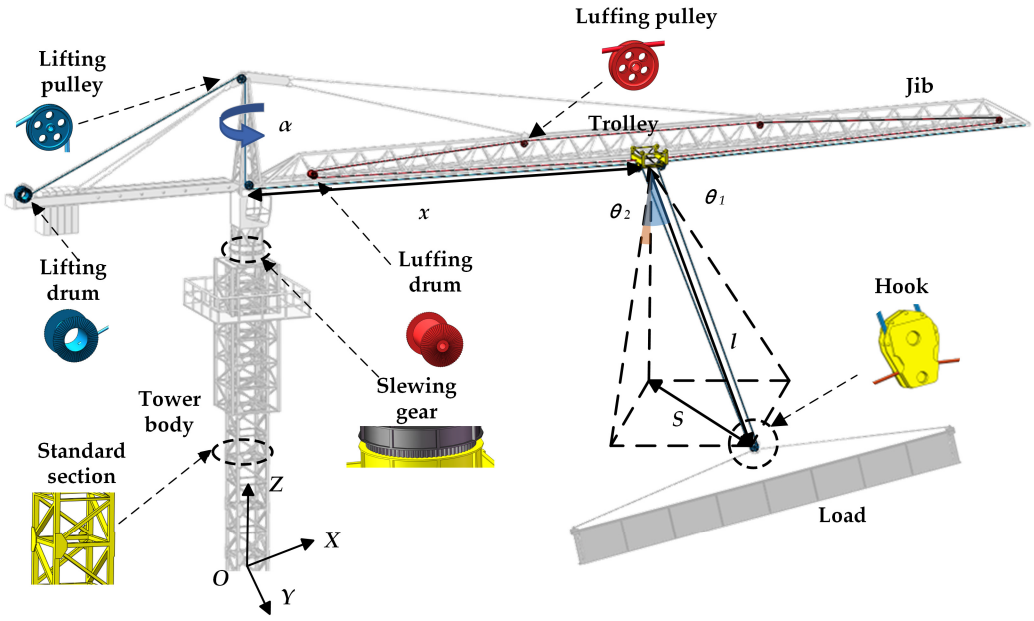


Figure 3. 3-D structure model.

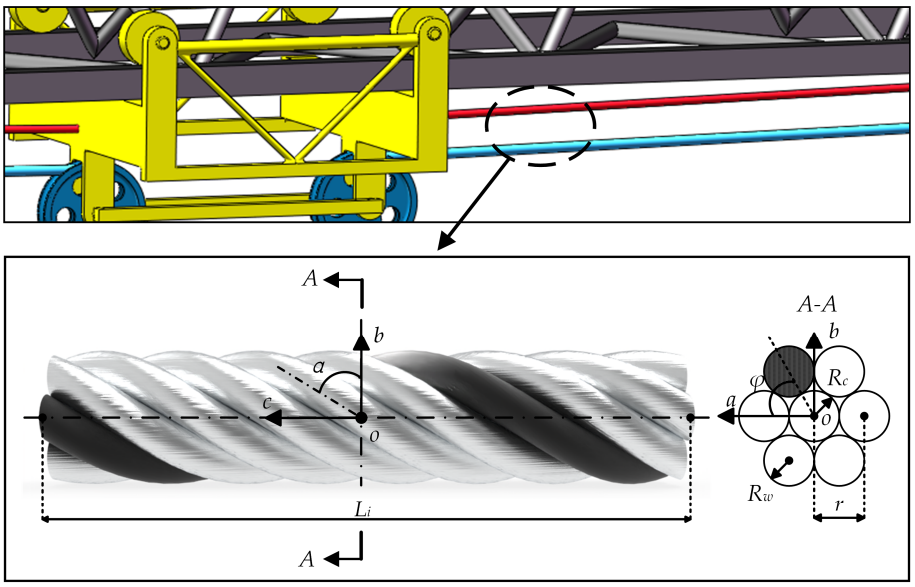


Figure 4. Wire rope model.

Figure 4 shows the structure of the wire rope used in the crane tower and its cross-section. The geometric parameters of the cross-section are as follows: R_c denotes the radius of the centerline of the wire rope. R_w denotes the diameter of the outer steel wire of the wire rope. r denotes the radius of a single steel wire in the wire rope. φ denotes the relative angle between adjacent wires to the center of the section.

3. Multibody Dynamical Model

Simscape Multibody contains a library of multibody dynamics modules for physical system modeling and corresponding simulation functions, which make the model highly descriptive of the actual system [25]. The multibody dynamics model of the tower crane is shown in Figure 5, where the parameters for the simulation images, which help clarify the modeling ideas, are taken from the tables in Section 3.1 to follow, and the software used is MATLAB 2022a.

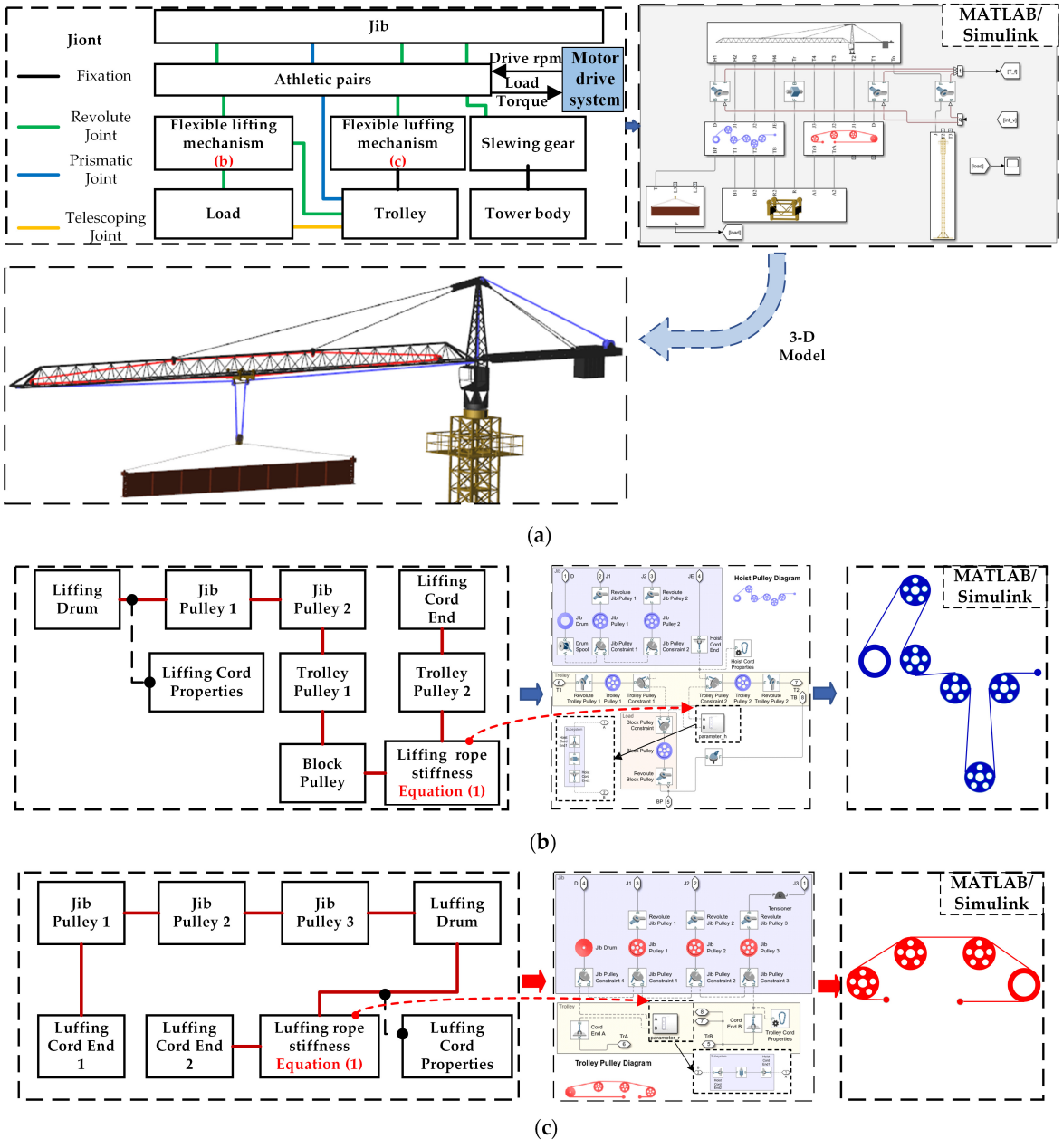


Figure 5. Multibody dynamics model: (**a**) overall structure; (**b**) flexible lifting mechanism; (**c**) flexible luffing mechanism.

Figure 5a shows the overall structure of the multibody dynamics model, in which the rigid bodies are built by recognizing the parameter information of the SolidWorks 2018 model and combining it with the geometry module of multibody dynamics [26]. The rigid bodies are coupled and assembled through the joint module and the rope-pulley module. In this model, the flexible lifting mechanism and the flexible luffing mechanism control the lifting and luffing motions of the tower crane during work, respectively. Specifically, as shown in Figure 5b, the rope-pulley of the flexible lifting mechanism is wound with double single strands. The wire rope and the hook pulley form a dynamic pulley block structure, and the two ends of the wire rope are connected to the reel and the end of the boom, respectively. As shown in Figure 5c, the rope-pulley of the flexible luffing mechanism is wound with a single strand of wire. The two ends of the wire rope are fixed on both sides perpendicular to the direction of movement of the dolly, and the pulleys are all fixed pulleys. The lifting and the luffing rope stiffness modules are used to set the wire rope stiffness coefficient, which can accurately simulate the physical properties and deformation of the wire rope in actual operation.

2.1.2. Electrical Subsystem

The model of the motor drive system is shown in Figure 6. The control method adopts closed-loop frequency conversion control. The control section generates PWM signals according to the speed feedback and reference speed trajectory, and the PWM signals are amplified by the inverter bridge to drive the induction motor to rotate, and the torque is output through the speed reducer. The lower half of Figure 6 shows the model established on the MATLAB 2022a software platform, from which the internal logical relationships and structure of the model can be seen, with all parameters as shown in Table 2 of Section 3.1.

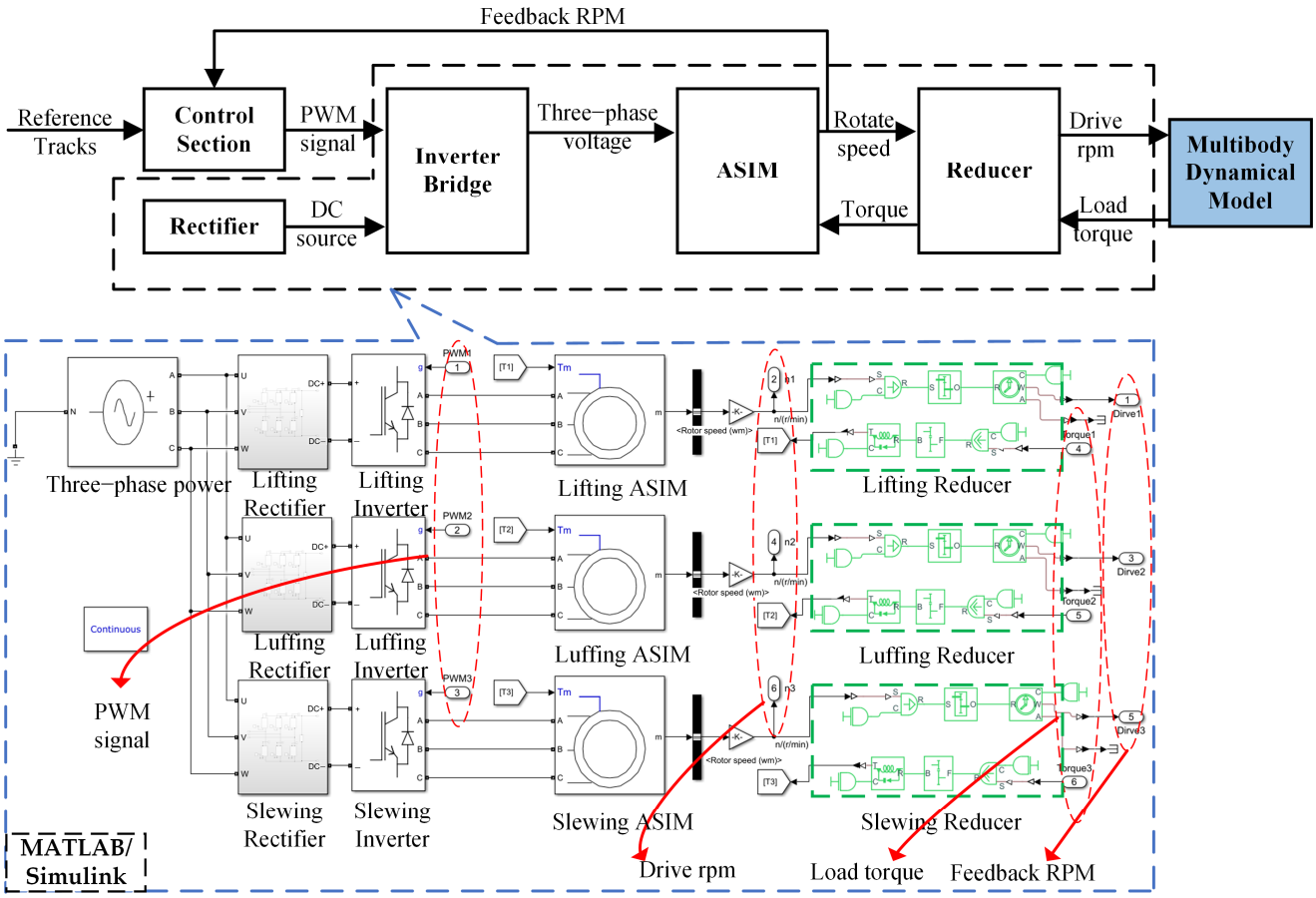


Figure 6. Motor drive system.

The system is mainly composed of two parts: the gear motor and the controller. The gear motor includes the induction motor and the speed reducer, and the controller is composed of the rectifier physical module, the inverter bridge, and the control section. The control section adopts the variable-voltage inverter closed-loop speed regulation method, as shown in Equations (3)–(7). Equations (3)–(5) calculate the voltage and frequency based on the speed error, and Equations (6) and (7) generate the PWM signal.

$$e_i = n_{\mathrm{refi}} - n_i, i = 1, 2, 3 \tag{3}$$

$$U_i = (k_{\mathrm{P}i} e_i + k_{\mathrm{I}i} \int e_i \mathrm{d}t) / f_0, \tag{4}$$

$$f_i = 2\pi (k_{\mathrm{P}i} e_i + k_{\mathrm{I}i} \int e_i \mathrm{d}t), \tag{5}$$

$$\begin{bmatrix} U_{Ui} \\ U_{Vi} \\ U_{Wi} \end{bmatrix} = U_i \begin{bmatrix} \sin(\int 2\pi f_i \mathrm{d}t) \\ \sin((\int 2\pi f_i \mathrm{d}t) - 2\pi/3) \\ \sin((\int 2\pi f_i \mathrm{d}t) + 2\pi/3) \end{bmatrix} \tag{6}$$

$$\begin{cases} U_{Ui}{}' = P(U_{Ui}, Q) \\ U_{Vi}{}' = P(U_{Vi}, Q) \\ U_{Wi}{}' = P(U_{Wi}, Q) \end{cases} \tag{7}$$

Included among these:

$$P(U, Q) = \begin{cases} 1, Q > U \\ -1, Q \le U \end{cases}$$

$$Q = \begin{cases} -1 + \frac{4}{T} t, (\frac{kT}{2} \le t \le \frac{(k+1)T}{2}, k = 0, 1, 2, \ldots) \\ 3 - \frac{4}{T} t, (\frac{(k+1)T}{2} \le t \le \frac{(k+2)T}{2}, k = 0, 1, 2, \ldots) \end{cases}$$

where: the subscripts i = 1, 2, 3 denote the lifting, luffing, and slewing drive motors respectively. t is the time. n_{refi} is the reference speed. n_i is the feedback rotation speed. e_i is the rotational speed error, and $k_{\mathrm{p}i}$ and $k_{\mathrm{I}i}$ are the proportional and integral gains respectively. f_0 is the fundamental frequency. U_i is the RMS phase voltage, and f_i is the stator phase voltage frequency. U_{Ui}, U_{Vi}, and U_{Wi} denote the three-phase sinusoidal voltage signals, and $U_{Ui}{}'$, $U_{Vi}{}'$, and $U_{Wi}{}'$ represent the corresponding PWM signals. $P(U, Q)$ is the comparative function. Q is the bipolar triangular carrier function in a period, and T is the carrier period.

2.2. Sensitivity Analysis of Operating Parameters

In this paper, the Sobol sensitivity analysis method is used to obtain for the first time the degree of contribution of different operating parameters to the effect of load swing during the operation of a tower crane. The method is based on multiple integral decomposition, which is used to obtain the influence index of the coupling between parameters, and the parameter range can be extended to the whole parameter domain [27,28]. Among the system response indexes used in the sensitivity analysis method, which is commonly used nowadays, none can reflect the change in wire rope length. Considering that the length of the wire rope in the flexible transmission mechanism is constantly changing, and the offset distance contains information on the rope length, this paper uses the maximum value of offset distance to characterize the load swing and accurately assess the degree of load swing in different operation stages.

The following assumptions were made using the Sobol sensitivity analysis: (1) any two sets of operating parameters are statistically uncorrelated. (2) the output of the model is a single value: the offset distance.

The steps of the Sobol sensitivity analysis method are as follows:

Step 1: The input parameters are obtained by Optimized Latin Hypercube Sampling, and two samples with capacity p are taken, which are represented by matrices $\boldsymbol{A}_{p\times n}$ and $\boldsymbol{B}_{p\times n}$, where p is the number of input parameters, and n is the number of parameter levels.

Step 2: The matrix $\boldsymbol{C}_i$ is the replacement of column i of matrix $\boldsymbol{A}$ ($i \leq 8$) with column i of matrix $\boldsymbol{B}$, leaving the remaining columns unchanged. Similarly, the matrix $\boldsymbol{C}_{-i}$ is the replacement of column i of matrix $\boldsymbol{B}$ ($i \leq 8$) with column i of matrix $\boldsymbol{A}$, leaving the remaining columns unchanged. Each group of operating parameters in matrices $\boldsymbol{C}_i$ and $\boldsymbol{C}_{-i}$ is substituted into the model for calculation respectively, and the output response values corresponding to each group of operating parameters are obtained. The variance estimation of the system response and parameter sensitivity indexes are obtained by the Monte Carlo algorithm. The calculation process is shown in Equation (8)~(14):

$$\hat{f}_0^2 = \frac{1}{n}\sum_{r=1}^{n} f_A(x_{r1},\ldots,x_{rp}) f_B(x'_{r1},\ldots,x'_{rp}) \tag{8}$$

$$\hat{V}^2 = \frac{1}{n}\sum_{r=1}^{n} f_A^2(x_{r1},\ldots,x_{rp})^2 - \hat{f}_0^2 \tag{9}$$

$$\hat{U}_i = \frac{1}{n}\sum_{r=1}^{n} f_A(x_{r1},\ldots,x_{rp}) f_{C_i}(x_{r1},\ldots,x_{r(i-1)},x'_{ri},x_{r(i+1)},\ldots,x_{rp}) \tag{10}$$

$$\hat{U}_{-i} = \frac{1}{n}\sum_{r=1}^{n} f_A(x_{r1},\ldots,x_{rp}) f_{C_{-i}}(x'_{r1},\ldots,x'_{r(i-1)},x_{ri},x'_{r(i+1)},\ldots,x'_{rp}) \tag{11}$$

$$D_{x_i} = (\hat{U}_i - \hat{f}_0^2)/\hat{V} \tag{12}$$

$$D_{x_i}^{\mathrm{T}} = 1 - (\hat{U}_{-i} - \hat{f}_0^2)/\hat{V} \tag{13}$$

$$D_{x_i}^{\mathrm{I}} = \left| D_{x_i}^{\mathrm{T}} - D_{x_i} \right| \tag{14}$$

In the equation both f_A and f_B are the outputs of the model, x_{r1} to x_{rp} are the elements of matrix $\boldsymbol{A}$, $x_{r1}{}'$ to $x_{rp}{}'$ are the elements of matrix $\boldsymbol{B}$, and $\hat{f}_0^2$, $\hat{V}^2$, $\hat{U}_i$ and $\hat{U}_{-i}$ are intermediate quantities. The local index D_{x_i} describes the effect of a single variable on the output, reflecting the magnitude of the first-order sensitivity. The global index $D_{x_i}^{\mathrm{T}}$ of input parameter x_i, contains the main effect of the variable and the interaction of this variable with the remaining variables, reflecting the magnitude of global sensitivity. The difference between the global index and the local index is the interactive index. The larger the interactive indexes $D_{x_i}^{\mathrm{I}}$ the more significant the interactions. The dominant parameters and the interactive parameters are screened out by the global indexes and interactive indexes.

The subsequent analysis is based on the minimum values of the operating parameters as shown in Table 3 of Section 3.1. The velocity trajectory consists of three phases: acceleration phase, uniform velocity phase, and deceleration phase. The initial position of the trolley is set to be 10 m from the center of the tower body, and the direction of the luffing motion is in the direction away from the center of the tower body.

As in Figure 7, through progressive calculation, the sensitivity level tends to stabilize when n is greater than 5000, so the sample number is taken as 5000.

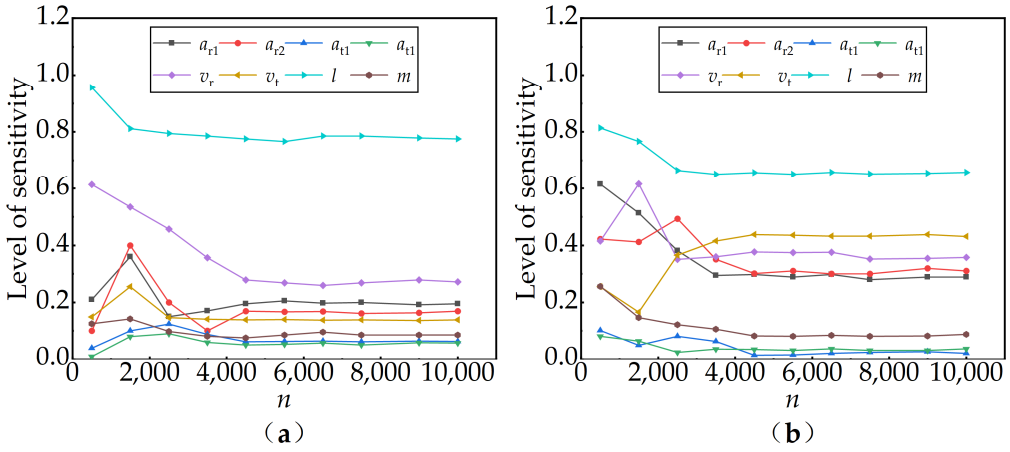


Figure 7. Variation of offset distance sensitivity indexes with sample number: (**a**) local sensitivity index; (**b**) global sensitivity index.

3. Results and Discussion

3.1. Model Validation

Since the MATLAB 2022a/Simulink software environment can integrate multiple physical domains, in this section, the EMRFC model of the QTZ55 tower crane is constructed in this environment with the flexible transmission mechanism as the core and the motor drive system as the driving force, combining physical modeling and mathematical modeling.

The main parameters needed of the EMRFC model are shown in Tables 1 and 2, where the parameters are derived from the parameter configuration of the QTZ55 tower crane as well as from the literature [24].

Table 1. Material properties of Q235 steel.

Operating Parameter	Value	Unit
Densities	7850	kg/m^3
Yield strength	375	MPa
Tensile strength	235	MPa
Modulus of elasticity	200	GPa
Elongation	25	%

Table 2. The main parameters of the EMRFC model.

Name	Notation	Value	Unit
Carrier period	T	10×10^{-4}	s
Core cross-section	A_{c1}, A_{c2}	3.32×10^{-5}, 0.75×10^{-5}	m^2
Core diameter ratio	ξ	1	/
Core radius	R_{c1}, R_{c2}	3.25×10^{-3}, 1.55×10^{-3}	m
Core wire cross Section	A_{w1}, A_{w2}	3.32×10^{-5}, 0.75×10^{-5}	m^2
Drum Diameter	D_d	0.254	m
Drum mass	D_m	145	kg
Elastic modulus	E_0	1.8×10^{11}	Pa
Gear ratio	N_1, N_2, N_3	15.9, 90, 195	/
Helix angle	α_1, α_2	57, 62	deg
Initial lifting rope Length	L_1'	126	m
Jib end distance	H_1	57	m
Jib inertia	J	1.02×10^7	kg·m^2
Jib tail distance	H_2	12.4	m

Table 2. *Cont.*

Name	Notation	Value	Unit
Logarithmic	p_1, p_2, p_3	4, 3, 3	/
Luffing rope length	L_2	183	m
Moment of inertia	J_1, J_2, J_3	2.2, 1.8, 3.6	kg·m^2
Number of cores	N	6	/
Poisson's ratio	ν	0.3	/
Pulley Diameter	P_{d}	0.381	m
Pulley mass	P_{m}	18.35	kg
Rated power of motor	$P_{\mathrm{N1}}, P_{\mathrm{N2}}, P_{\mathrm{N3}}$	5.4×10^3, 4×10^3, 11×10^3	W
Reference length	L_0	0.2	m
Rotational damping	B_1, B_2, B_3	0.0252, 0.023, 0.0852	N·m·s/deg
The sum of the core radius	r_1, r_2	6.5×10^{-3}, 3.1×10^{-3}	m
Trolley quality	M_1	324	kg
Trolley quality	M_1	324	kg
Twisting radius	R_{w1}, R_{w2}	3.25×10^{-3}, 1.55×10^{-3}	m
Wire strain	$\varepsilon_{w1}, \varepsilon_{w2}$	0.0686, 0.533	%

The wire rope models used for the lifting and luffing mechanisms in the QTZ55 tower crane are 6 × 37-13-1670-I and 6 × 19-6.2-1670-I, respectively, according to the configuration parameters.

The required ranges of operating parameters refer to the QTZ55 tower crane configuration parameters, as shown in Table 3.

Table 3. Range of values for operating parameters.

Operating Parameter	Notation	Minimum Value	Maximum Value
Luffing up-acceleration	a_{r1} (m/s^2)	0.1	0.5
Luffing down-acceleration	a_{r2} (m/s^2)	0.1	0.5
Luffing speed	v_{r} (m/s)	0.5	1
Slewing up-acceleration	a_{t1} (deg/s^2)	0.5	2.5
Slewing down-acceleration	a_{t2} (deg/s^2)	0.5	2.5
Slewing speed	v_{t} (deg/s)	2	4
Lifting height	l (m)	10	30
Load mass	m (kg)	1000	3000

To verify the accuracy of the model, the load swing process under the composite working condition (luffing-slewing condition) of the EMRFC model, the traditional dynamic equation model [29], and the QTZ55 tower crane were compared, and the data of the QTZ55 tower crane were obtained from the literature [30]. The slewing and luffing speeds were set to be 1.2 deg/s and 0.5 m/s respectively, the slewing and luffing accelerations were 0.24 deg/s^2 and 0.1 m/s^2, respectively, the running time was 30 s, and the radial and tangential swing angles started from 0 and −1.5 deg, respectively. These settings are derived from the actual working parameters of the QTZ55 tower crane.

Figure 8 shows the swing process of the load for the composite working condition. Table 4 summarizes the swing process errors of the EMRFC model and the traditional dynamics equation model for the QTZ55 tower crane. From Figure 8a–c and Table 4, the errors of the EMRFC model are smaller, and the trend of load swing of the EMRFC model is closer. From Figure 8d–f, with the improvement of load quality, the offset distance curves of the QTZ55 tower crane and EMRFC model change consistently, while the traditional kinetic equation model is almost unchanged, which shows that EMRFC model considering

flexible transmission characteristics can more accurately describe the load swing process. Meanwhile, it can also be noticed that the larger the load mass, the larger the swing.

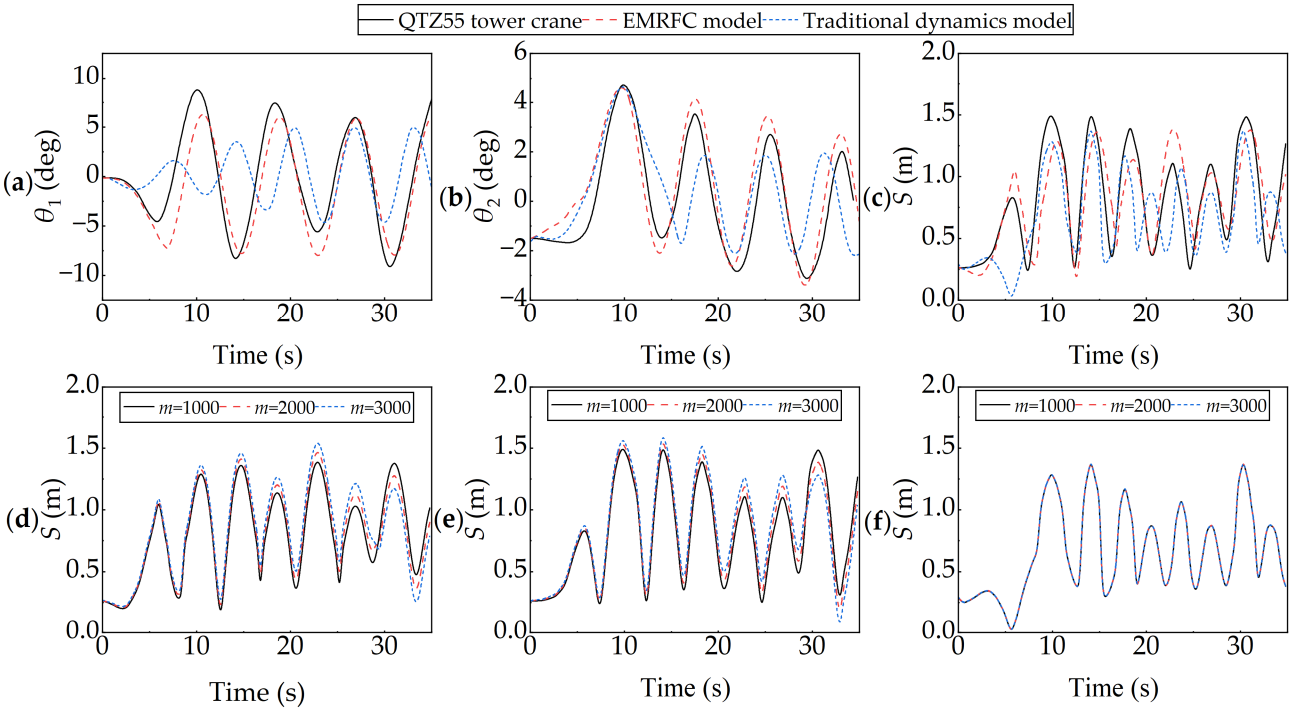


Figure 8. Swing process of the load: (**a**) radial swing angle; (**b**) tangential swing angle; (**c**) offset distance; (**d**) QTZ55 tower crane for different load quality; (**e**) EMRFC model for different load quality; (**f**) traditional dynamics equation model for different load quality.

Table 4. Error statistics of the models.

Model	The Average Error of Radial Swing Angle/%	The Average Error of Tangential Swing Angle/%	The Average Error of Offset Distance/%
EMRFC	7.2	1.17	2.81
Traditional dynamics model	15.2	1.8	8.3

The results show that the EMRFC model comprehensively considers the electrome chanical-rigid-flexible coupling effect of the tower crane. The accuracy of the prediction of the load motion is higher, which can be used as the basis for the study of the load swing law under the composite working condition.

3.2. Impact of Flexible Transmission Characteristics on Load Swing

The transmission wire rope is an important force component in the flexible transmission of the tower crane, and its stiffness will directly affect the swing of the tower crane load, while the elastic modulus (E) of the wire rope is a key factor in determining its stiffness [31]. Therefore, this section analyzes the effect of different elastic modulus on the load offset distance from the perspective of time and frequency domains. To characterize the load swing, the whole working period is divided into two phases according to the deceleration endpoint: the running phase (0~30 s) and the stopping phase (30~90 s).

Figure 9 shows the impact of different E on load swing. From Figure 9a, with the increase of E, the offset distance in the running phase gradually decreases, and the offset distance in the parking phase gradually increases. Notably, the offset distance in the stopping phase of the swing shows the phenomenon of "beat vibration". This phenomenon is

due to the load swing in space during the stopping phase. This swing is decomposed into radial and tangential components by mutually perpendicular planes. From Figure 9b, the main frequencies of these two angles are close to each other, respectively 0.13611 Hz and 0.14875 Hz, with a frequency difference of only 0.013 Hz, which will cause the two pendulum angles to excite each other, so that the offset distance curve exhibits the phenomenon of "beat vibration". In addition, as shown in Figure 9c, as the modulus of elasticity increases, the main frequency difference between the pendulum angle components becomes smaller and smaller, which increases the frequency of the beat vibration. This special vibration imposes additional shaking moments and torques on the structure of the tower and the drive motor respectively. Therefore, the stiffness of the wire rope on the load swing is not to be ignored. The parameters design of intelligent control for tower cranes that overlook the nonlinear impact of wire rope stiffness on the swing of loads in the flexible drive will affect control precision.

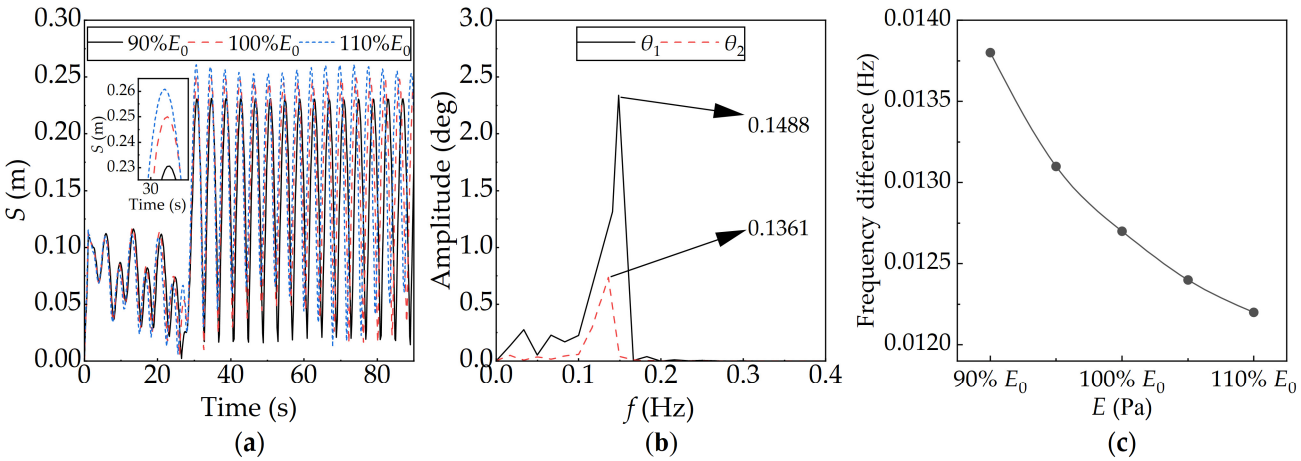


Figure 9. Impact of different E on load swing: (**a**) offset distance curve; (**b**) swing angle amplitude-frequency curves of 100%E; (**c**) main frequency difference.

3.3. Impact of Operating Parameters on Load Swing

3.3.1. Sensitivity Analysis of Operating Parameters on Load Swing

Figure 10 depicts the indexes of sensitivity of each operating parameter on the load swing at different stages. The operating parameters have different indexes of sensitivity on the load swing at different stages, in which the global index of l is the largest, which is 0.66 and 0.95, respectively. The average local index, average global index, and interaction index are also calculated, and the summarized data are shown in Table 5. The data show that using the average global index of 0.05 as the dividing line, the dominant operating parameters affecting the load offset distance are l, v_t, v_r, a_{r1}, a_{r2}, and m. The parameters with significant interactions can be derived from the size of the interaction index as l, v_t, v_r.

Table 5. Average sensitivity indices of operating parameters.

Operating Parameter	Average Local Index/ $\bar{D}_{x_i}$	Average Globe Index/$\bar{D}^{T}_{x_i}$	Interactive Index/$\bar{D}^{I}_{x_i}$
l	0.64	0.79	0.15
v_r	0.25	0.31	0.07
v_t	0.09	0.17	0.08
a_{r1}	0.17	0.16	0.01
a_{r2}	0.15	0.14	0.01
m	0.06	0.07	0.01
a_{t1}	0.08	0.05	0.03
a_{t2}	0.06	0.05	0.01

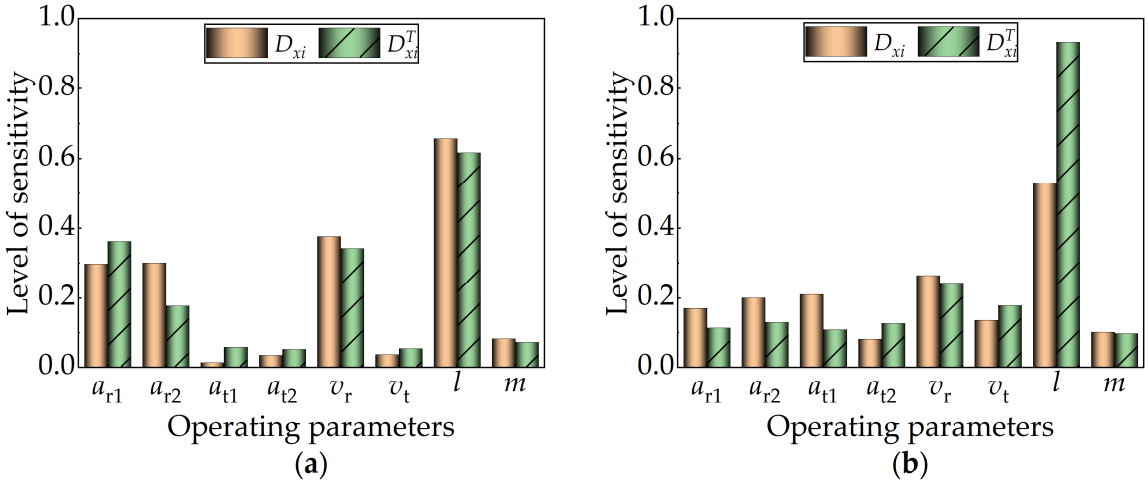


Figure 10. Sensitivity analysis of operating parameters: (**a**) running phase; (**b**) stopping phase.

3.3.2. Impact of Dominant Operating Parameters on Load Swing

To study the impact characteristics of dominant operating parameters on load swing, this paper uses the control variable method to set the values of different dominant operating parameters in sequence, obtaining the index curve of load offset distance as shown in Figure 11. Furthermore, Table 6 counts the maximum offset distances and cycles of the loads during the running and stopping phases for different operating parameters, as well as the "beat vibration" cycles during the stopping phase.

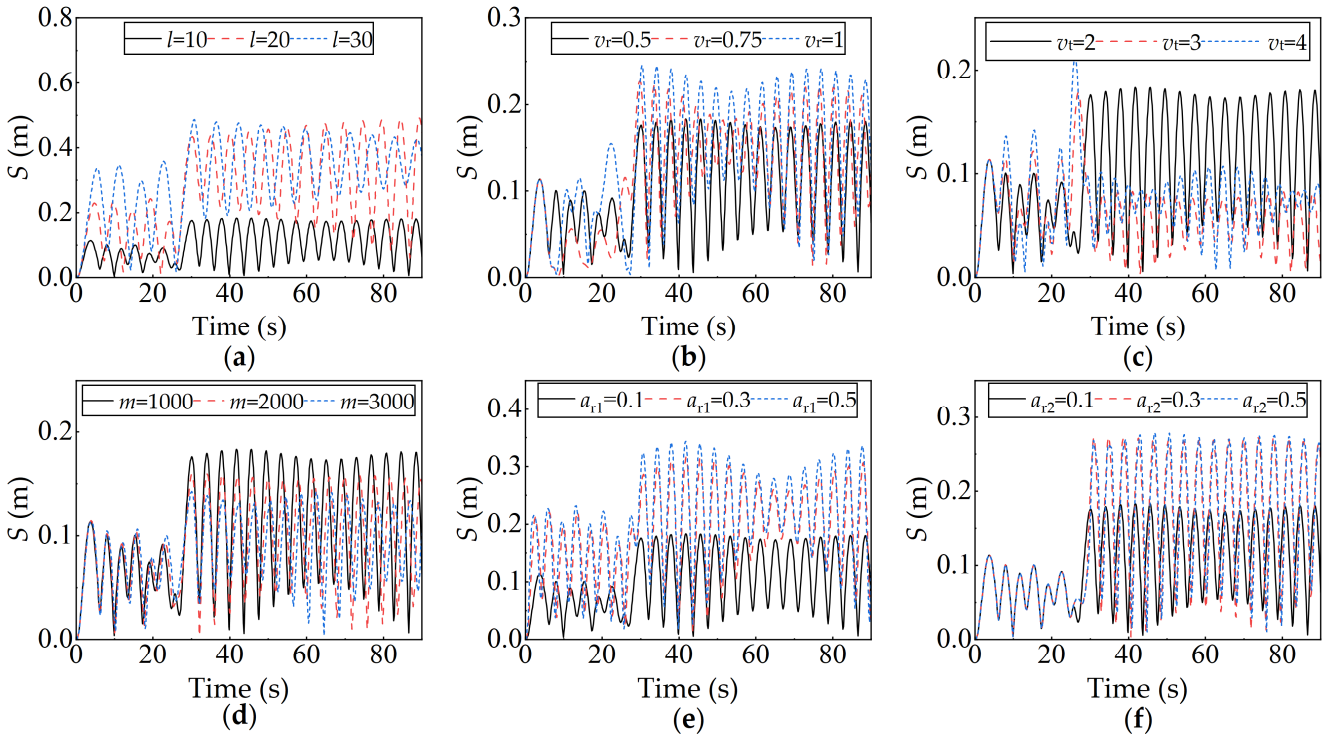


Figure 11. Curve of load offset distance under different operating parameters conditions: (**a**) lifting height; (**b**) luffing speed; (**c**) slewing speed; (**d**) load mass; (**e**) luffing up-acceleration; (**f**) luffing down-acceleration.

Table 6. Maximum value and period of the offset distance under different operating parameter conditions.

Operating Parameter	Value	Running Phase		Stopping Phase		
		Maximum Offset Distance/m	Period/s	Maximum Offset Distance/m	Period/s	Period of Beat Vibration/s
l (m)	10	0.12	6.34	0.18	6.34	50
	20	0.24	7.92	0.44	8.03	50
	30	0.35	10.05	0.49	10.02	50
v_r (m/s)	0.5	0.12	6.34	0.18	6.34	50
	0.75	0.12	6.18	0.23	6.12	50
	1.0	0.16	6.27	0.26	6.15	50
v_t (deg/s)	2	0.12	6.34	0.18	6.34	50
	3	0.17	6.51	0.82	6.31	40
	4	0.23	6.48	0.11	6.33	30
a_{r1} (m/s^2)	0.1	0.12	6.34	0.18	6.34	50
	0.3	0.22	5.68	0.32	6.31	50
	0.5	0.23	5.84	0.35	6.37	50
a_{r2} (m/s^2)	0.1	0.12	6.34	0.18	6.34	50
	0.3	0.12	6.34	0.27	6.32	50
	0.5	0.12	6.34	0.28	6.31	50
m (kg)	1000	0.12	6.34	0.18	6.34	50
	2000	0.13	6.33	0.13	6.31	45
	3000	0.14	6.34	0.11	6.29	40

In both Figure 11 and Table 6, the offset distance in the stopping phase increases significantly with the increase in the lifting height, and the offset distance period in this phase is 6.38 s, 8.03 s, and 10.02 s, which is basically in accordance with the period formula of the single pendulum, $T = 2\pi\sqrt{l/g}$. There are some differences because the lifting mechanism is a dynamic pulley mechanism, not an ideal single pendulum. Luffing speed significantly increases the load offset distance but does not affect the swing period. It is interesting to note that as slewing speed increases, the offset distance initially increases during the running phase and then decreases rapidly during the stopping phase, and the "beat vibration" period decreases linearly. As the load mass increases, the offset distance increases during the running phase, decreases during the stopping phase, and the "beat vibration" period decreases linearly. As the luffing up-acceleration increases, the offset distance increases rapidly because the higher the up-acceleration, the higher the mechanical energy of the load at the end of acceleration, the higher the potential energy of the load at zero velocity, and thus the larger the offset distance. As the luffing down-acceleration increases, the offset distance increases rapidly during the stopping phase due to the sudden change in acceleration, so the velocity trajectory of the deceleration process can be replaced by a smoother velocity trajectory.

From the above analysis, we can find that the period of the offset distance is only affected by l, and the period of the "beat vibration" is affected by m and v_t. In addition, compared with the running phase, the offset distance in the stopping phase is larger, because the load and the trolley are moving in the running phase, and the relative motion between them is small, after the trolley stops, the load continues to swing due to the inertia, and at this time, the relative motion between the trolley and the load is larger. The offset distance in the stopping phase exhibits a tendency to increase with the increase of l, a_{r1}, and a_{r2}, and the offset distance in the stopping phase exhibits linear positive correlation, linear negative correlation, and linear positive correlation, with the increase of v_r, m, and v_t, respectively. This is because the tower crane system is nonlinear, its dynamic behavior

is complex and difficult to describe by a simple linear relationship, which is also why the current intelligent control of the tower crane is difficult. In addition, based on the results of the sensitivity analysis in the previous section, a_{t1}, a_{t2}, and m can be adjusted individually, so that a_{r1} and a_{r2} as 0.1 m/s^2, m as 1000~3000 kg can be set with less fluctuation in the offset distance. From the control point of view, the tower crane's intelligent control realizes precise lifting by adjusting the operation parameters. Therefore, the driving motor can be guided to drive the tower crane actuating end according to the above influence law to achieve precise lifting.

3.3.3. Impact of Interactive Operating Parameters on Load Swing

From the analysis above, it is known that the interactive operating parameters include l, v_t, v_r. The maximum offset distances S_1 and S_2 in the running and stopping phases are taken as the indicators of the load swing. The effects of the combination of lifting height l, the luffing speed v_r, and the slewing speed v_t on S_1 and S_2 are investigated.

Figure 12 shows the contour distributions of the peak offset values in the running and stopping phases for different luffing speeds and slewing speeds. From Figure 12a, the change of S_1 is more complicated. When v_t is less than 3 m/s, S_1 increases firstly and then decreases with the increase of v_r. When v_t is more than 3 m/s, S_1 increases first and then decreases with the increase of v_r, and then increases rapidly, because the contribution of the luffing motion to the system response is enhanced under the condition of high slewing speed, however, when the luffing speed is further increased, the system's nonlinear response either reaches a new equilibrium state, resulting in the offset distance firstly decreasing and then rapidly increasing at higher luffing speeds. From Figure 12b, it can be seen that S_2 decreases or increases with the increase of v_r or v_t, respectively, and in particular, within the luffing variable speed range [0.5~0.6 m/s, 0.9~1.0 m/s] and slewing variable speed range [2.5~3.0 deg/s], the tower crane system exhibits a more stable dynamic response with a smaller peak offset of load swing. Therefore, by adjusting the motor drive parameters to match these optimal operating intervals, the swing problem caused by the nonlinear response of the system can be significantly reduced to ensure the safety and stability of the system during the acceleration and deceleration phases.

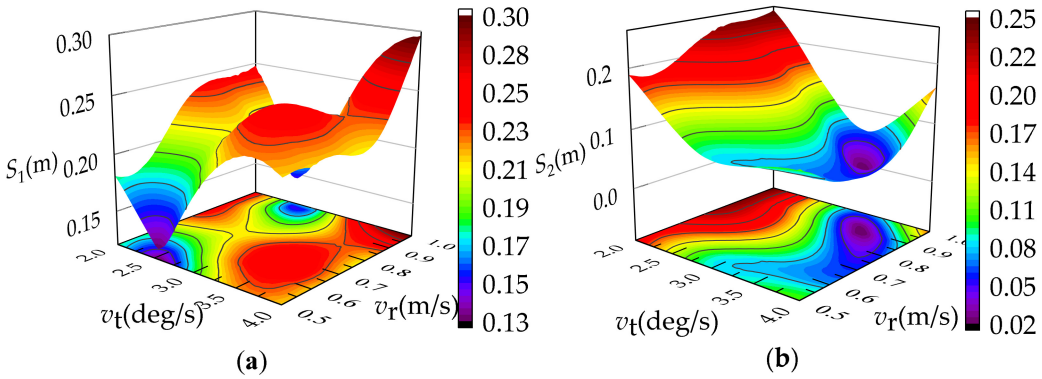


Figure 12. Interaction analysis of luffing speed and slewing speed: (**a**) running phase; (**b**) stopping phase.

Figure 13 shows the contour distributions of the offset peaks in the running and stopping phases at different luffing speeds and lifting heights. The contour plots of Figure 13a,b show a similar trend, with S_1 and S_2 having a significant step increase with the increase of l. Especially at l of 14 m, there is a significant turn in the change of S_1 and S_2. When l is in the range of 25~30 m, S_1, and S_2 increase significantly, indicating that the interaction between l and v_r is significantly elevated in this range, so the tower crane should avoid working

in the range of l of 25~30 m and v_r is 0.65~1.0 m/s. Especially in intelligently controlled tower cranes, the system can effectively circumvent these unfavorable operating ranges by monitoring and adjusting parameters in real time.

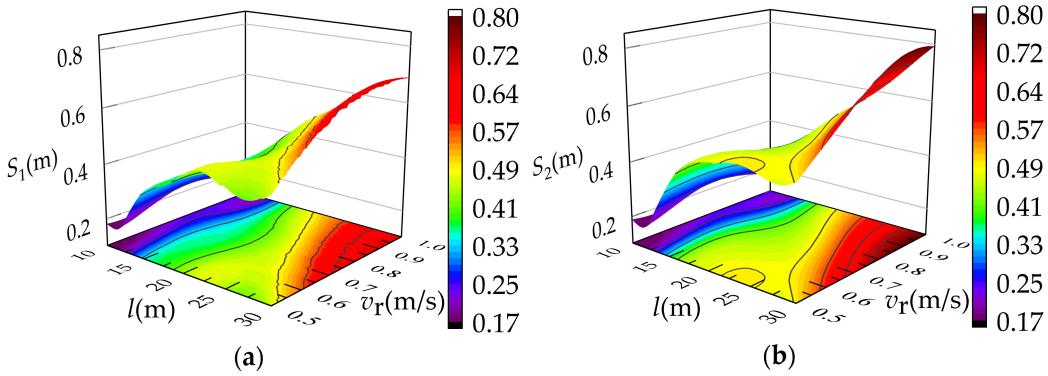


Figure 13. Interaction analysis of luffing speed and lifting height: (**a**) running phase; (**b**) stopping phase.

Figure 14 shows the contour distributions of the maximum values of the offset distances in the running and stopping phases at different lifting heights and slewing speeds. From Figure 14a, when l is less than 25 m, the change of S_2 is relatively smooth; when l is 25~30 m, S_2 increases rapidly, especially when S_1 is certain, l and v_t show a negative correlation. It can be seen from Figure 14b, that S_2 increases with the increase of l, showing a "saddle" distribution; when l is in the range of 25~30 m, S_2 increases rapidly, this is due to the lifting height being larger, the load swing having a greater linear velocity, which is subjected to the greater centripetal force, resulting in the load to produce a greater swing amplitude.

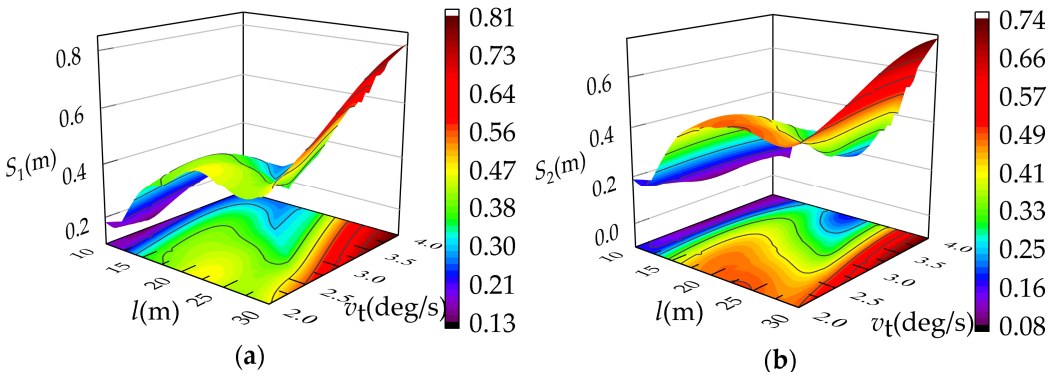


Figure 14. Interaction analysis of slewing speed and lifting height: (**a**) running phase; (**b**) stopping phase.

The analysis of Figures 12–14 shows that the load offset distance shows a complex trend under different parameter combinations, so attention should be paid to the impact of their interaction on load swing in the adjustment of operating parameters. Through the analysis of the contour plot, the adjustment of the operating parameters such as luffing speed, slewing speed, and lifting height helps to keep the variation of the offset distance within a small range. Therefore, setting l, v_r, and v_t to [10~15 m], [0.5~0.6 m/s, 0.9~1.0 m/s], and [2.5~3.0 deg/s], respectively, can limit the offset distance to less than 0.2 m, which reasonably improves the working accuracy.

4. Conclusions

To deeply investigate the influence mechanism of multiple operating parameters interactions on the load swing of tower cranes, the EMRFC model for the QTZ55 was built in this paper. Based on the model in this paper, the impact of wire rope elasticity on load swing is discussed. The dominant and interactive operation parameters affecting the load swing are determined by the Sobol sensitivity analysis method, and the impact of dominant and interactive parameters on offset distance is analyzed. The main conclusions are as follows:

- This paper takes multibody dynamics as a bridge to effectively couple electric drive, mechanical structure, and flexible transmission, and establishes the EMRFC model for the QTZ55 tower crane. The model accurately describes the nonlinear effects of the rigid-flexible coupling and electromechanical coupling on the load swing of the tower crane, and the modular modeling makes the model easy to extend.
- The elasticity of the wire rope of the flexible drive mechanism affects the swing amplitude of the load, and the swing amplitude of the load in the running and stopping phases increases and decreases, respectively, when the mass of the load is increased. In addition, the amplitude of the load swing increases as the modulus of elasticity of the wire rope increases, and a "beat vibration" phenomenon is commonly observed during the stopping phase.
- The interaction among the lifting height, slewing speed, and luffing speed has a significant effect on the load offset distance; the offset distance shows a complex trend with the increase of the slewing speed and luffing speed, and shows a step change trend with the increase of the lifting height.
- The reasonable ranges for various operating parameters of the tower crane are given under the composite working conditions. Setting the operating parameters a_{r1} and a_{r2} as 0.1 m/s^2, a_{t1} and a_{t2} as 0.5~2.5 deg/s^2, l as 10~15 m, v_r as [0.5~0.6 m/s, 0.9~1.0 m/s], m as 1000~3000 kg, and v_t as 2.5~3.0 deg/s, the offset distance can be limited to 0.2 m.

Based on the research findings of this paper, on the one hand, it can accurately simulate the actual operation process of tower cranes, and on the other hand, determining the reasonable range of operating parameters is a prerequisite for the intelligent control of tower cranes. It provides a data foundation for intelligent decision support systems, helping decision-makers formulate reasonable decisions and strategies, improving the accuracy and reliability of decision outcomes, and enhancing their performance and safety under complex working conditions.

In future work, research will continue the intelligent control methods for swing suppression that consider the actual transmission process of tower cranes, in order to enhance efficiency and safety in tower crane engineering applications.

Author Contributions: Conceptualization, P.L. and Y.S.; methodology, C.Z.; software, X.Z.; validation, C.Z., Y.S. and X.Z.; formal analysis, X.Z.; investigation, P.L.; resources, Y.S.; data curation, C.Z.; writing—original draft preparation, C.Z.; writing—review and editing, P.L.; visualization, C.Z.; supervision, Y.S.; project administration, P.L.; funding acquisition, Y.S. All authors have read and agreed to the published version of the manuscript.

Funding: This work was supported by National Natural Science Foundation of China (51505049), Shaanxi Provincial Natural Science Basic Research Program (2024JC-YBMS-428).

Data Availability Statement: Data can be obtained from the corresponding author upon reasonable request.

Conflicts of Interest: The authors declare no competing interests.

Appendix A

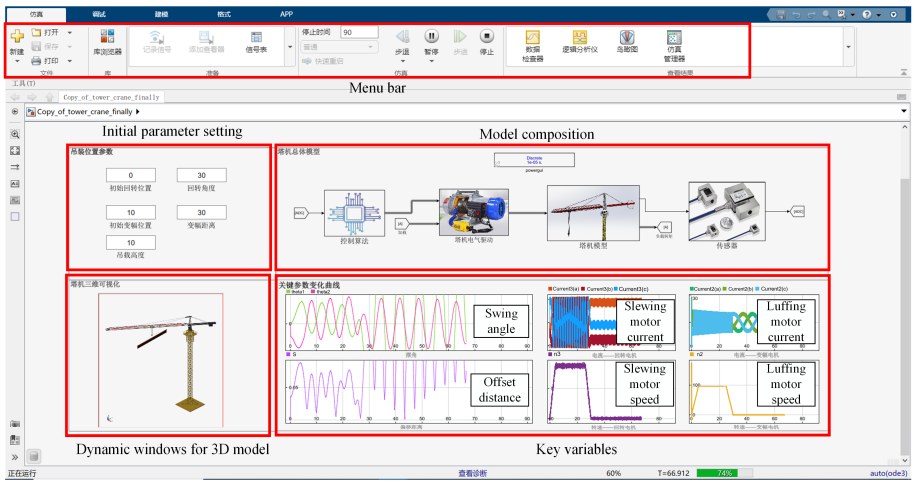


Figure A1. The EMRFC model in the MATLAB 2022a/Simulink software.

References

1. Hu, S.; Fang, Y.; Bai, Y. Automation and optimization in crane lift planning: A critical review. *Adv. Eng. Inform.* **2021**, *49*, 101346. [CrossRef]
2. Ramli, L.; Mohamed, Z.; Abdullahi, A.M.; Jaafar, H.; Lazim, I. Control strategies for crane systems: A comprehensive review. *Mech. Syst. Signal. PR.* **2017**, *95*, 1–23. [CrossRef]
3. Zheng, Z.; Wang, F.; Gong, G.; Han, D. Intelligent technologies for construction machinery using data-driven methods. *Automat. Constr.* **2023**, *147*, 104711. [CrossRef]
4. Zhu, H.; Hwang, B.; Asce, M.; Ngo, J.; Tan, J. Applications of smart technologies in construction project management. *J. Constr. Eng. M.* **2022**, *148*, 0002260. [CrossRef]
5. Kolawach, C.; Shuichiro, H.; Hiroshi, Y. Vibration reduction of the rotary crane with flexible boom. *J. Mech. Eng.* **2022**, *9*, 22–31.
6. Tong, Z.; Wu, W.; Guo, B.; Zhang, J.; He, Y. Cargo swing analysis and swing angle optimization of flat-top tower cranes. *J. Vib. Eng. Technol.* **2023**, *12*, 4715–4727. [CrossRef]
7. Jiang, W.; Ding, L.; Zhou, C. Digital twin: Stability analysis for tower crane hoisting safety with a scale model. *Automat. Constr.* **2022**, *138*, 104257. [CrossRef]
8. Montonen, J.H.; Nevaranta, N.; Niemelä, M.; Lindh, T. Comparison of extrainsensitive input shaping and swing-angle-estimation-based slew control approaches for a tower crane. *Appl. Sci.* **2022**, *12*, 5945. [CrossRef]
9. Liu, F.; Yang, J.; Wang, J.; Liu, C. Swing characteristics and vibration feature of tower cranes under compound working Condition. *Shock. Vib.* **2021**, *2021*, 8997396. [CrossRef]
10. Liu, F.; Yang, J.; Wang, J.; Liu, C.D.; Liu, C. Effect on tower crane structural vibration under the lifting-luffing coupling condition. *J. Mech. Sci. Technol.* **2023**, *37*, 4935–4947. [CrossRef]
11. Peng, J.; Huang, J.; Singhose, W. Payload twisting dynamics and oscillation suppression of tower cranes during slewing motions. *Nonlinear. Dyn.* **2019**, *98*, 1041–1048. [CrossRef]
12. Cao, X.; Yang, Y.; Wang, W.; Gu, Z. Rigid-Flexible coupling dynamic modeling of a tower crane with long flexible boom. *Mech. Mach. Sci.* **2017**, *55*, 39–57.
13. Cheng, B.; Yang, B.; Wang, D.; Duan, M. Finite element analysis of complete structure of tower cranes. *J. Phys. Conf. Ser.* **2023**, *2419*, 012004. [CrossRef]
14. Zhang, M.; Zhang, Y.; Ji, B.; Ma, C.; Cheng, X. Modeling and energy-based sway reduction control for tower crane systems with double-pendulum and spherical-pendulum effects. *Meas. Control* **2020**, *53*, 141–150. [CrossRef]
15. Feng, R.; Zhang, E.; Dong, M. Jib vibration and payload swing of tower cranes in the case of trolley motion. *Arab. J. Sci. Eng.* **2021**, *46*, 12179–12191. [CrossRef]
16. Li, K.; Liu, M.; Yu, Z.; Lan, P.; Lu, N. Multibody system dynamic analysis and payload swing control of tower crane. *Proc. Inst. Mech. Eng. Part K J. Multi-Body Dyn.* **2022**, *236*, 407–421. [CrossRef]
17. Florentin, R.; Oliver, S. Modeling and control of tower cranes with elastic structure. *IEEE. Trans. Control Syst. Technol.* **2020**, *236*, 64–79.
18. Zhou, Y.; Meng, Z. An improved negative zero vibration anti-swing control strategy for grab ship unloader based on elastic wire rope model. *Mec. Ind.* **2021**, *22*, 45.

19. Gu, J.; Qin, Y.; Xia, Y.; Jiao, Q. Research on dynamic characteristics of composite towering structure. *Int. J. Appl. Mech.* **2021**, *13*, 2150096. [CrossRef]
20. Wei, Y.; Hu, T.; Yue, P.; Luo, W.; Ma, S. Study on the construction theory of digital twin mechanism model for mechatronics equipment. *Int. J. Adv. Manuf. Tech.* **2022**, *131*, 5383–5401. [CrossRef]
21. Jiao, Q.; Li, B.; Qin, Y.; Wang, F.; Gu, J.; Wang, J.; Mi, C. Research on dynamic characteristics of lifting rope-breaking for the nuclear power crane. *J. Fail. Anal. Prev.* **2021**, *21*, 1220–1230. [CrossRef]
22. Shi, H.; Tao, F.; Tong, S.; Tang, Y.; Han, G. Research on nonlinear coupled tracking controller for double pendulum gantry cranes with load hoisting/lowering. *Nonlinear Dyn.* **2022**, *108*, 223–238. [CrossRef]
23. Viacheslav, L.; Yuriy, R.; Liubov, S.; Yuriy, L. The dynamic analysis of the joint trolley movement and hoisting mechanism in the tower crane. *Strength Mater. Theory Struct.* **2022**, *108*, 267–282.
24. De Menezes, E.A.W.; Marczak, R.J. Comparative analysis of different approaches for computing axial, torsional and bending stiffnesses of cables and wire ropes. *Eng. Struct.* **2021**, *241*, 112487. [CrossRef]
25. Pozzi, M.; Achilli, G.; Valigi, M.; Malvezzi, M. Modeling and simulation of robotic grasping in simulink through simscape multibody. *Front. Robot. AI.* **2022**, *9*, 873558. [CrossRef] [PubMed]
26. Boschetti, G.; Sinico, T. Designing digital twins of robots using simscape multibody. *Robotics* **2024**, *13*, 62. [CrossRef]
27. Mao, Z.; Luo, Y.; Zhou, S. The multi-objective optimisation design of outlet guide vanes of diagonal flow fan based on Sobol sensitivity analysis. *Proc. Inst. Mech. Eng. Part A J. Power Energy* **2024**, *238*, 382–400. [CrossRef]
28. Zhou, R.; Feng, W.; Deng, Z.; Gao, H.; Ding, L.; Li, N. Parameter sensitivity analysis and main parameter estimation of wheel-ground mechanical model. *Chin. J. Aeronauts.* **2021**, *42*, 253–265.
29. Tian, Z.; Yu, L.; Huimin, O.; Zhang, G. Swing suppression control in tower cranes with time-varying rope length using real-time modified trajectory planning. *Automat. Constr.* **2021**, *132*, 103954. [CrossRef]
30. Liu, X. Study on the Vibration Characteristics of Crane Arm Under Slewing Condition of Tower Crane. Master's Thesis, Shandong Jianzhu University, Jinan, China, 2023.
31. Qin, Z.; Huang, Q.; Jin, H.; Xue, H. Simulation of multi-body dynamics and strand stress analysis of hoisting wire rope. *J. Notrhwest. Polytechnical. Univ.* **2020**, *38*, 485–493. [CrossRef]

Disclaimer/Publisher's Note: The statements, opinions and data contained in all publications are solely those of the individual author(s) and contributor(s) and not of MDPI and/or the editor(s). MDPI and/or the editor(s) disclaim responsibility for any injury to people or property resulting from any ideas, methods, instructions or products referred to in the content.